Journal of Ceramic Processing Research. Vol. 25, No. 6, pp. 937~940 (2024)
(Received 29 March 2024, Received in revised form 2 November 2024, Accepted 15 December 2024)
https://doi.org/10.36410/jcpr.2024.25.6.937

J O U R N A L O F
Ceramic Processing Research

Electrochemical and structural properties of carbon-coated $LiFe_{0.2}Mn_{0.8}PO_4$ cathode

Ung Jae Jeon[a,†], Tae-Yeon Shim[a,†], In-Ho Im[c,*], Kyong-Nam Kim[b,*] and Seung-Hwan Lee[a,*]
[a]*Department of Battery Convergence Engineering, Kangwon National University, Chuncheon 24341, Republic of Korea*
[b]*Department of Semiconductor Engineering, Daejeon University, Daejeon 34520, Republic of Korea*
[c]*Department of Electrical Engineering, Shinansan University, Ansan 15435, Republic of Korea*

Olivine-structured $LiFePO_4$ is anticipated as a promising cathode material for lithium-ion batteries and lithium polymer batteries. In our research group, we synthesized homogeneous and fine particles of $LiFePO_4$ and $LiFe_{0.2}Mn_{0.8}PO_4$ using mechanical alloying (MA) to address the low electrical conductivity and lithium ion diffusion rate of $LiFePO_4$. $LiFe_{0.2}Mn_{0.8}PO_4$ exhibited similar structural characteristics to $LiFePO_4$, yet it demonstrated superior electrochemical properties. It achieved a capacity of 159.4 mAh/g, an electrical conductivity of 4.9×10^{-7} S/cm, excellent cycle and rate performance, and a lithium ion diffusion coefficient of 2.1×10^{-14} cm^2 S^{-1}. These findings highlight the effectiveness of mechanical alloying in enhancing the electrochemical performance of $LiFePO_4$-based materials, paving the way for their application in advanced lithium-ion battery technologies.

Keywords: $LiFePO_4$, $LiFe_{0.2}Mn_{0.8}PO_4$, Electrical conductivity, Lithium ion diffusion coefficient.

Introduction

Lithium-ion secondary batteries have become a cornerstone for powering a wide array of devices, from IT products to energy storage systems, and notably, electric vehicles (EVs). The cathode material, a critical component of these batteries, has traditionally been dominated by transition metal oxides with layered structures like $LiCoO_2$ (LCO). LCO-based compounds are prized for their excellent charging and discharging properties, respectable capacity, and relatively high voltage characteristics. However, they are not without their drawbacks, primarily due to the use of Co and Ni. They are expensive relative to other transition metals, also raises environmental concerns due to its toxicity in case of Co.

This backdrop has spurred a significant amount of research into finding alternative cathode materials that can match or exceed the performance of LCO without its disadvantages. Much of this research has concentrated on improving the capacity and cycle life of cathodes operating at around 4 V (3.7~3.9 V). A breakthrough came when olivine-type cathode materials were introduced. In 1997, the group led by Professor Goodenough at the University of Texas unveiled a pioneering study. They demonstrated that electrochemical reactions for lithium ions were viable in olivine-structured transition metal phosphates, which are based on the polyanion $[PO_4]^{3-}$. This discovery paved the way for the development of $LiFePO_4$ (LFP), a material that supersedes traditional layered cathode materials like LCO by substituting Co with Fe phosphate. This substitution not only achieves a structure of high stability, known as the olivine structure but also positions LFP as a leading cathode material for lithium-ion batteries. LFP's attributes, including its high power output, affordability, low toxicity, superior thermal stability, and excellent reversibility, make it an exceptionally promising candidate.

LFP is noted for its remarkable thermal stability, a result of the strong covalent bonds between phosphorus and oxygen atoms, which effectively prevent the release of oxygen and thus contribute to its overall stability as a cathode material. As a result, batteries employing LFP as the cathode material have found widespread application in the electric vehicle sector, especially in electric buses and hybrid electric vehicles (HEVs).

In the current study, we have taken a step further by doping LFP with manganese (Mn), which has led to a significant enhancement in both its structural stability and electrochemical performance. The effects of Mn doping in LFP are as follows: 1) it shortens the lithium ion migration pathway in the LFP crystal structure, facilitating the insertion and extraction of lithium ions; 2) it enhances electronic conductivity; and 3) it

*Corresponding author:
Tel : +82-33-250-6265
E-mail: shlee@kangwon.ac.kr, knam1004@dju.kr, iminho@sau.ac.kr
[†]These authors contributed equally.

lowers the activation energy required for the insertion and extraction of lithium ions. Especially, the addition of Mn reduces structural changes during the lithium insertion and extraction processes of LFP, which helps facilitate lithium ion movement over the long term, thereby enhancing cycle performance. This improvement underscores the potential of Mn-doped LFP in advancing the capabilities of lithium-ion batteries, making them more suitable for a wider range of applications, including more demanding environments and longer life cycles.

Experimental

To synthesize $LiFe_{0.2}Mn_{0.8}PO_4$ (LFMP), we utilized lithium hydroxide monohydrate ($LiOH{\cdot}H_2O$, Aldrich, ≥98%) as the lithium source. Iron(III) oxide (Fe_2O_3, Aldrich, ≥99%) and ammonium dihydrogen phosphate ($(NH_4)_2HPO_4$, Aldrich, ≥99%) served as the sources of iron and phosphate, respectively, while acetylene black acted as the reducing agent. Manganese dioxide (MnO_2, Aldrich, ≥99%) was selected as the transition metal source for doping. The process involved mechanical alloying using a shaker type ball miller (SPEX 8000M) equipped with a hardened steel vial set (Vial size 2¼ in., containing two 1/2 in. and four 1/4 in. steel balls). We meticulously loaded the starting materials in stoichiometric proportions based on the chemical reaction formula and performed ball milling at a speed ranging from 1000 to 1050 rpm for 2 hours. This was done under both wet (with isopropyl alcohol) and dry conditions to establish the most effective milling environment. The ratio of powder to balls was carefully adjusted between 5:1 and 20:1, all while maintaining an argon atmosphere to prevent oxidation.

The crystal structure of the synthesized materials was determined using X-ray diffraction (XRD) with a CuKα source (40 kV, 100 mA, Rigaku D-MAX3000), scanning from 10° to 70° 2θ at a rate of 5°/min. Particle morphology and distribution were examined with a field emission scanning electron microscope (JEOL). For the electrochemical testing, we prepared the cathode material by blending the synthesized active material with a conductive agent (Acetylene Black) and binder (Polytetrafluoroethylene) in a 75:20:5 wt.% ratio. This mixture was then further homogenized in an agate mortar with isopropyl alcohol as a dispersant for over 10 minutes, resulting in a dough-like substance. This mixture was spread onto a stainless steel mesh (Exmet) to act as the current collector and then compressed to form electrodes with an active material area of 1 cm^2 (20 mg/cm^2). The electrodes were subsequently vacuum-dried at 120°C for 12 hours or more.

Lithium metal (FMC, 99.9%) with a thickness of 0.15 mm was used as the anode to assemble a 2-electrode half-cell, incorporating a porous polypropylene film as the separator. The electrolyte comprised 1M $LiPF_6$ dissolved in a 1:1 volume mixture of ethylene carbonate (EC) and dimethyl carbonate (DMC) (Merck). The entire cell assembly process was conducted in a Glove Box (VAC Co.) under an argon atmosphere with less than 1 ppm of moisture to ensure purity. Electrochemical properties were evaluated using a battery tester (Maccor 4000-series), where charge/discharge characteristics and cycling performance were assessed. The cut-off voltage ranged from 2.5 to 4.3 V, and charge/discharge rates varied from 0.1 C to 10 C rate, allowing us to thoroughly analyze the material's performance under various conditions.

Result and Discussion

Fig. 1(a) presents the X-ray diffraction (XRD)

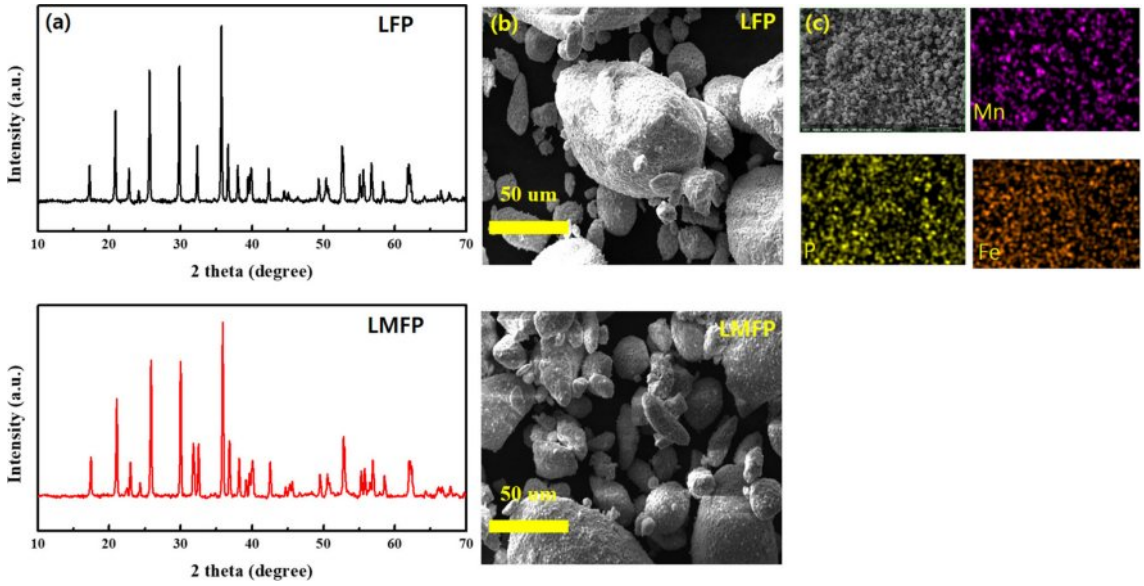

Fig. 1. (a) XRD patters, (b) SEM images of LFP and LMFP, (c) EDS mapping of LMFP.

observations illustrating the effects of Mn substitution on LFP and LFMP. It was observed that regardless of the substitution, all samples exhibited the characteristic Olivine structure of the intended materials. Notably, no secondary phases such as Li_3PO_4 or $Li_3Fe_2(PO_4)_3$, which could arise from compositional heterogeneity during synthesis, were detected in any of the samples. Additionally, there were no discernible impurities stemming from the substitution elements. Moving on, Fig. 1(b) showcases scanning electron microscope (SEM) images of the synthesized LFP and LFMP materials. These images provide visual insights into the morphology and surface characteristics of the materials, revealing any potential differences between the two compositions. Furthermore, Fig. 1(c) displays the results of electron dispersive X-ray analysis (EDX) mapping conducted on LMFP powder. This analysis was performed to verify the distribution and state of Mn substitution within the $LiFePO_4$ structure. The EDX mapping confirms that Mn is uniformly dispersed throughout the $LiFePO_4$ matrix, indicating successful substitution and uniform distribution within the material. Based on structural properties, the combination of XRD, SEM imaging, and EDX mapping provides comprehensive characterization of the structural and compositional properties of the synthesized LFP and LFMP materials, confirming the successful incorporation of Mn and the preservation of the Olivine structure in both compositions.

Fig. 2 depicts the initial discharge capacities of both LFP and LFMP. In the case of LFMP, where Mn substitutes for Fe, the initial discharge capacity notably increases to 159.4 mAh/g, surpassing that of LFP, which stands at 157.1 mAh/g. This slight improvement in discharge capacity can be attributed to several factors. Firstly, the measured electrical conductivity of the powders provides insights into the enhanced performance of LFMP. The electrical conductivity of LFP is measured at 8.1×10^{-8} S/cm, while LFMP exhibits a significantly higher electrical conductivity of 4.9×10^{-7} S/cm. This approximately tenfold increase in electrical conductivity in LFMP compared to LFP suggests improved charge transfer kinetics within the electrode material. The enhanced electrical conductivity facilitates more efficient electron transport during the charge/discharge processes, leading to a higher discharge capacity. Furthermore, the substitution of Mn for Fe in LFMP could potentially influence the structural and electrochemical properties of the material. Mn substitution may introduce favorable structural modifications, such as increased lattice strain or enhanced lithium ion diffusion pathways, which can contribute to improved electrochemical performance. Additionally, Mn substitution could lead to the formation of defects or vacancies within the crystal structure, which may enhance lithium ion mobility and facilitate faster charge transfer kinetics. The Li-ion diffusion coefficient of LMFP in our paper is approximately 2.97×10^{-10} cm²/s.

To observe the cycling characteristics of each powder, cycle tests were conducted, and the results are presented in Fig. 3. For samples containing Mn, an initial capacity of 147.3 mAh/g was recorded at a 0.5 C, while LFP exhibited an initial capacity of 138.2 mAh/g after 200 cycles. As the cycling progressed, a slight increase in discharge capacity was observed for both samples. The gradual increase in capacity observed over cycles can be attributed to several factors. Initially, during the early cycles, larger particles within the electrode material may impede the movement of lithium ions, resulting in a relatively lower discharge capacity. The addition of Mn reduces structural changes during the lithium insertion and extraction processes of LFP, which helps facilitate lithium ion movement over the long term, thereby enhancing cycle performance. However, as the cycling progresses, these larger particles tend to stabilize, providing pathways for lithium ion movement. Consequently, the observed increase in capacity can be attributed to the stabilization of the electrode structure such as reduced lattice deformation and increase in contact area between the particles over cycles, facilitating improved lithium ion transport. In contrast, pristine LFP exhibits degradation behavior as the cycling progresses. This degradation may be attributed to several factors, including structural changes, particle aggregation, and electrode-electrolyte interactions, which can lead to decreased lithium ion diffusion rates and increased polarization. As a result, the discharge capacity of

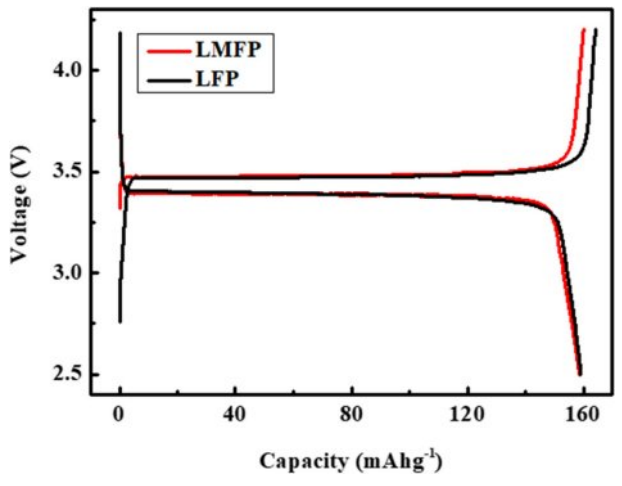

Fig. 2. Initial charge/discharge curves of LFP and LMFP.

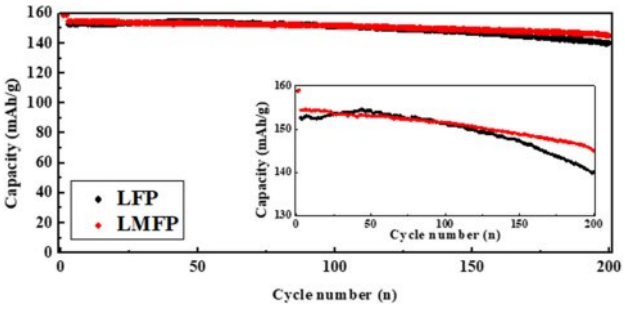

Fig. 3. Cyclability of LFP and LMFP.

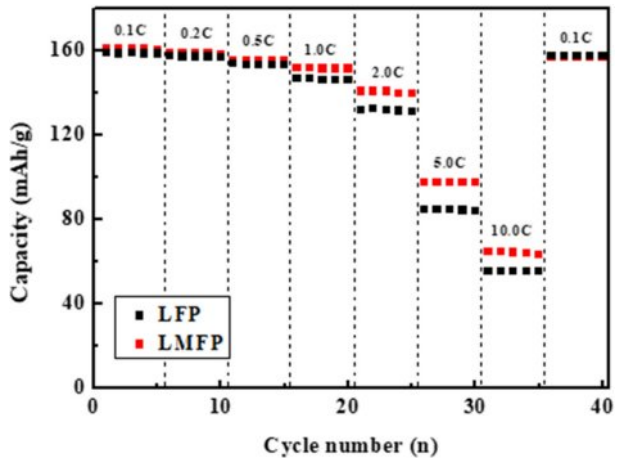

Fig. 4. Rate capability of LFP and LMFP.

pristine LFP tends to deteriorate over cycles.

Fig. 4 presents the rate-performance measurements for both samples. In the case of LFMP, a discharge capacity of 99.6 mAh/g was observed at a 5.0 rate, while at a 10.0 C rate, it exhibited a discharge capacity of 65.7 mAh/g. In contrast, for LFP without Mn, the discharge capacity was 82.6 mAh/g at a 5.0 C rate and decreased to 55.7 mAh/g at a 10.0 C rate. This reduction in overall capacity and lower high-rate discharge performance compared to LFMP was evident. Due to manganese substitution, the lattice structure changes, shortening the lithium ion pathways. This not only optimizes the lithium ion transport but also enhances the electronic conductivity by improving the electron conduction pathways, leading to better performance. It is well-known that the diffusion of lithium ions in lithium transition metal oxides determines the rate-limiting step during electrochemical reactions. The speed of lithium ion movement during electrochemical reactions is influenced by particle size. This phenomenon is related to the lithium ion diffusion coefficients, which for LMFP and LFP are 2.1×10^{-14} and 8.9×10^{-15} cm^2 S^{-1}, respectively. The improved diffusion coefficient observed in LFMP can be attributed to the partial substitution of Fe^{2+} (0.92 Å) at the 4c site with Mn^{2+} (0.97 Å), leading to a slight increase in lattice constants. This change in lattice constants increases the lattice volume within the LFP structure, facilitating the insertion/removal diffusion of Li ions. Additionally, this alteration in lattice volume acts as a structural scaffold, preventing changes in the Li ion diffusion volume.

Conclusion

In this paper, we focused on the synthesis and comparative analysis of LFP and LFMP cathode materials for lithium-ion batteries. We observed that LFMP exhibited superior electrochemical performance compared to LFP, particularly in terms of its diffusion coefficient. This enhanced performance can be attributed to the presence of Mn substitution, which results in an expansion of the lattice volume. This expanded lattice structure facilitates more facile insertion and extraction of lithium ions during the charge-discharge process, leading to improved diffusion kinetics and overall electrochemical performance. Thus, the incorporation of Mn into the LFP structure represents a promising strategy for enhancing the performance of lithium-ion battery cathode materials.

Competing Interests

The authors declare that they have no competing interests.

References

1. X. Zhang, M. Hou, A.G. Tamirate, H. Zhu, C. Wang, and Y. Xia, J. Power Sources 448 (2020) 227438.
2. D. Ding, Y. Maeyoshi, M. Kubota, J. Wakasugi, K. Kanamura, and H. Abe, J. Power Sources 449 (2020) 227553.
3. S. Oukahou, M. Maymoun, A. Elomrani, K. Sbiaai, and A. Hasnaoui, ACS Appl. Energy Mater. 5 (2022) 10591.
4. Q. Deng, T. Li, J. Wang, S. Zhang, H. Yang, C. Xu, and M. Wu, Ceram. Int. 50 (2024) 13702.
5. Y. Li, B. Xing, Z. Wang, H. Zhang, Y. Liu, J. Jiang, S. Yang, and B. Li, ACS Appl. Energy Mater. 2022 (5) 10983.
6. C.Y. Su, C.Y. Wu, S.Y. Hsu, C.Y. Wu, and J.G. Duh, Mater. Lett. 272 (2020) 127880.
7. Y. Song, Y. Liu, and X. Ou, Ceram. Int. 46 (2020) 5069.
8. H. Hu, X. Liu, Y. Lei, J. Chen, L. Wu, Z. Li, J. Liu, and X. Wang, J. Energy Storage 79 (2024) 110198
9. C. Luo, Y. Jiang, X. Zhang, C. Ouyang, X. Niu, and L. Wang, J. Energy Chem. 68 (2022) 206.
10. C.Y. Nam, H. Kim, W. Jin, J.H. Seol, T.H. Kim, S.Y. Yoon, and S. Choi, J. Energy Storage 80 (2024) 110254.
11. J. Barrio, M. Volokh, and M. Shalom, J. Mater. Chem. A 8 (2020) 11075.
12. Z. Wang, H. Xu, Z. Liu, M. Jin, L. Deng, S. Li, and Y. Huang, J. Mater. Chem. A 11 (2023) 9057.
13. Z. Zhao, X. Zhang, P. Wang, I.M. Pateli, H. Gao, G. Wang, and T.S. Irvine, J. Mater. Chem. A 12 (2024) 1736.
14. Y. Zhang, M. Shahriar, and S. Hu, J. Mater. Chem. A 11 (2023) 11849.
15. M.B. Yadav, Y.I. Kim, and Y.T. Jeong, Trans. Electr. Electron. Mater. 25 (2024) 25.